Generation of Equal-Energy Orbital Angular Momentum Beams via Photopatterned Liquid Crystals

Peng Chen,[1] Shi-Jun Ge,[1] Ling-Ling Ma,[1] Wei Hu,[1,*] Vladimir Chigrinov,[2] and Yan-Qing Lu[1,†]

[1]*National Laboratory of Solid State Microstructures, Collaborative Innovation Center of Advanced Microstructures and College of Engineering and Applied Sciences, Nanjing University, Nanjing 210093, China*

[2]*Department of Electronic and Computer Engineering, Center for Display Research, Hong Kong University of Science and Technology, Clear Water Bay, Kowloon, Hong Kong 999077, China*

(Received 30 January 2016; revised manuscript received 13 March 2016; published 18 April 2016)

Orbital angular momentum (OAM) has been extensively studied to date and has become topical in the last few years due to its potential for increasing bandwidth in optical communications. The so-called Dammann vortex grating (DVG) can generate a series of equal-energy OAM beams and satisfactorily realize OAM parallel detection, an important challenge in this field. However, previously reported DVGs suffer from polarization sensitivity, low efficiency, or the lack of tunability and mode variety. Here, a design of liquid-crystal DVGs is proposed and demonstrated for the generation of various equal-energy OAM beams. The DVGs, featured by alternative orthogonally planar-aligned regions, are carried out via photopatterning technology. Beam arrays composed of arbitrary OAM modes, as well as two-dimensional ones, are generated in good quality and high efficiency. The liquid-crystal DVGs exhibit merits of excellent polarization independency, electrical switchability, and tunability. This supplies a promising approach towards OAM generation, manipulation, and detection.

DOI: 10.1103/PhysRevApplied.5.044009

I. INTRODUCTION

Orbital angular momentum (OAM) has attracted considerable attention over the past two decades [1–4]. One example of an OAM-carrying mode is the Laguerre-Gaussian (LG) beam [5,6], which has two indices: the azimuthal index (m, i.e., the topological charge) and the radial index (p). A LG beam is featured by a helical phase front with a singularity in the center, resulting in a donutlike intensity distribution with $p+1$ concentric rings and an OAM of $m\hbar$ per photon [5]. OAM adds a new degree of freedom to the manipulation of light, inspiring applications including optical tweezers [7,8], nanostructure fabrications [9], nonlinear optics [10], and quantum informatics [11–13]. Especially, due to the infinite number of OAM states, the capacity of optical communications systems can be drastically enhanced via OAM-based multiplexing [14–16] and demultiplexing [17,18] technology.

Dammann vortex grating (DVG) provides equal-energy distribution among all desired diffraction orders with specific OAM states [19–21]. It enables the individual modulation and simultaneous detection of OAM, and thus can satisfactorily realize OAM parallel detection (i.e., detecting multiple collinear OAM beams in parallel), which is an important challenge in OAM-based optical communications [19]. At present, DVGs are mainly fabricated on photoresists [19–21] or glass substrates [22] via microelectronic lithography, or accomplished by spatial light modulators [23,24]. However, these techniques suffer from several drawbacks. The former is static and only highly efficient for certain wavelengths, while the spatial light modulator is commonly polarization dependent, costly, and optically inefficient. Besides, just simple LG beams with integral m and zero p are demonstrated. These restrict the applications of DVGs. Therefore, it is of great significance to explore new approaches to generate broadband-suitable and polarization-insensitive OAM beam arrays in high efficiency, good quality, and flexible mode variety.

In this work, liquid-crystal (LC) DVG consisting of alternative orthogonally planar aligned (PA) regions is proposed. Various LC DVGs are demonstrated through photopatterning a polarization-sensitive alignment agent with a dynamic microlithography system. Beam arrays composed of arbitrary OAM modes carrying integral or fractional m with and without p, as well as two-dimensional arrays, are generated in high quality and good energy uniformity. Moreover, these DVGs exhibit advantages of electrical switching, polarization independency, and tolerance to the wavelength of incident light.

II. PRINCIPLE AND FABRICATION

Dammann gratings (DGs) can uniformly distribute light energy among all desired diffraction orders [25,26]. Each period of the DG is composed of certain binary phase regions of different widths [27,28]. By combining DGs

*huwei@nju.edu.cn
†yqlu@nju.edu.cn

with conventional fork gratings (i.e., DVGs), equal-energy OAM beams at designed diffraction orders can be obtained. The spiral phase of the OAM modes can be integrated with the blazed grating phase to obtain a phase distribution written as

$$\varphi = 2\pi x/\Lambda + m\phi, \tag{1}$$

where m denotes the topological charge, ϕ is the azimuthal angle, x represents the horizontal axis, and Λ is the pitch of the grating. For more general cases of the LG mode, a term corresponding to the radial index p should be introduced [29–31]. The phase distribution changes to

$$\varphi = 2\pi x/\Lambda + m\phi + \pi\theta[-L_p^{|m|}(2r^2/w_0^2)], \tag{2}$$

where $\theta(x)$ represents a unit step function, $L_p^{|m|}(x)$ represents the generalized Laguerre polynomial, and $r^2 = x^2 + y^2$ and w_0 represents the output beam-waist radius. Owing to the change of the sign of the associated Laguerre polynomial, there exist p circular discontinuities where the phase shifts by π. Therefore, the transmission function of a general DVG can be described as

$$T(x) = \sum_{n=-\infty}^{+\infty} C_n \exp\left(in \times \{2\pi x/\Lambda + m\phi + \pi\theta[-L_p^{|m|}(2r^2/w_0^2)]\}\right), \tag{3}$$

where the coefficient C_n of the nth order can be expressed as [32]

$$C_n = \begin{cases} \frac{-i}{2n\pi}\left[1 + 2\sum_{k=1}^{N-1}(-1)^k \exp(-i2\pi n x_k) + (-1)^N \exp(-i2\pi n x_N)\right] & n \neq 0 \\ 2\sum_{k=1}^{N-1}(-1)^k x_k + (-1)^N x_N & n = 0, \end{cases} \tag{4}$$

where $\{x_k\}$ are normalized phase transition points in one period with boundary values $x_0 = 0$ and $x_N = 1$, and N is the total number of transition points. $|C_n|^2$ is the power of the nth order normalized with respect to the total power. By optimizing the values of $\{x_k\}$, the light energy can be distributed into desired orders (M) with good uniformity and high efficiency. Accordingly, when the incident light passes through such a DVG, it will be diffracted into several desired orders with equally distributed energy carrying topological charge nm. Specially, due to the phase shift of $n\pi$, only odd orders possess a nonzero p.

The phase pattern of DVG can be obtained by binarizing a blazed spiral-phase distribution [Eq. (2)] into 0 and π phase values. By integrating two orthogonal one-dimensional DVGs [i.e., $\mathrm{mod}(\varphi_x + \varphi_y, 2\pi)$, where φ_x and φ_y are the binarized phase patterns of one-dimensional DVGs in x and y dimension, respectively], two-dimensional DVGs can be realized, which have the ability to create $M_x \times M_y$ spot array. In this work, DVGs with five desired diffraction orders are presented using normalized phase transition points within each period: $x_1 = 0.038\,63$, $x_2 = 0.390\,84$, and $x_3 = 0.655\,52$ [27]. The phase patterns of designed DVGs with $m = 1$, $m = 0.5$, and $m = 1$ and $p = 1$ are shown in Figs. 1(a), 5(a), and 5(d), respectively.

Such phase patterns (both one-dimensional and two-dimensional ones) can be realized by locally controlling the LC orientations due to its pronounced optical birefringence. As illustrated in Fig. 1(b), the phase pattern marked in the dashed line in Fig. 1(a) is formed by the orthogonal PA regions. Thanks to such a design, any incident light could be decomposed into two perpendicular components, polarized along the two alignment directions (x and y). Because of the refractive-index difference (Δn_x or Δn_y) between adjacent regions, phase retardation (Γ_x or Γ_y) will be induced. Δn_x and Δn_y can be described as

$$|\Delta n_x| = |\Delta n_y| = \Delta n_{\mathrm{eff}} = n_{\mathrm{eff}} - n_o, \tag{5}$$

where n_{eff} changes from n_e to n_o with an increasing voltage. Then, Γ_x and Γ_y are

$$|\Gamma_x| = |\Gamma_y| = \frac{2\pi(n_{\mathrm{eff}} - n_o)d}{\lambda}, \tag{6}$$

where d is the cell gap and λ is the wavelength of incident light. The two perpendicular components will experience the same phase retardation. Thereby, the diffraction efficiency is independent of incident polarization [33]. When $\Gamma = (2a+1)\pi$ (a is an integer), the LC DVGs can generate equal-energy OAM beams in the maximum efficiency (*on* state). While $\Gamma = 2a\pi$, the diffraction cannot occur (*off*

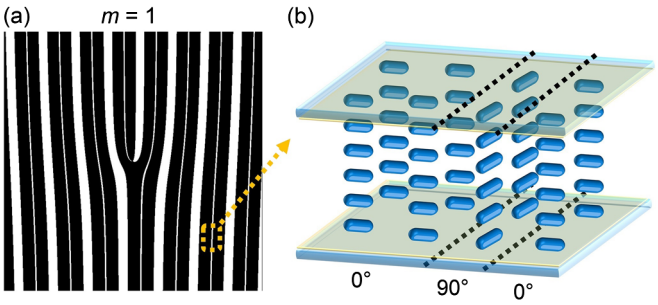

FIG. 1. (a) The phase pattern of a 1×5 DVG with $m = 1$, where black indicates 0 and white indicates π. (b) Schematic cell structure of the LC DVG, which is composed of alternative orthogonal PA regions.

state). The electro-optical tunability of LCs makes it possible to dynamically switch between *on*/*off* states and operate at different wavelengths.

Photoalignment is suitable for high-resolution multidomain LC alignments [34]. Here, a two-step photoexposure process [33] is performed to carry out the designed LC orientations through photopatterning via dynamic microlithography technology [35]. A polarization-sensitive and rewritable sulphonic azo-dye SD1 (Dai-Nippon Ink and Chemicals Inc., Japan) is used as the alignment agent. The SD1 molecules tend to reorient their absorption oscillators perpendicular to the UV light polarization and further guide the LC directors [36]. The excellent image output capability of this technique allows arbitrary LC orientations to be generated conveniently [37,38]. Two pieces of glass substrates spin coated with SD1 are assembled with 6-μm spacers and then sealed with epoxy glue to form the cell. Then it is placed at the image plane of the exposure system to record the patterns with certain polarization. Afterwards, filling the cell with LC E7 yields the designed DVGs.

III. RESULTS AND DISCUSSION

Figure 2 exhibits the micrographs of the fabricated LC DVG with $m = 1$ and the period $\Lambda \approx 130$ μm. Figures 2(a) and 2(b) show the cases that the incident polarization is parallel or perpendicular to the alignment directions. So the incident light does not change its polarization, and is blocked by the crossed analyzer while it totally passes through the parallel analyzer, indicating dark and bright states, respectively. For Figs. 2(c) and 2(d), the polarizer is fixed at 45° with respect to the alignment directions. In this case, the incident light satisfying the half-wave and full-wave condition can transmit the crossed and parallel analyzer [39], corresponding to the greenish and purplish states here. In all micrographs, any adjacent regions are quite uniform in color and brightness except for some boundary lines, which are related to the disclinations between the adjacent heterogeneous orientations [40]. The dispersed dark points are spacers for maintaining a uniform cell gap. The uniformity proves the high quality and excellent orthogonality of adjacent alignment.

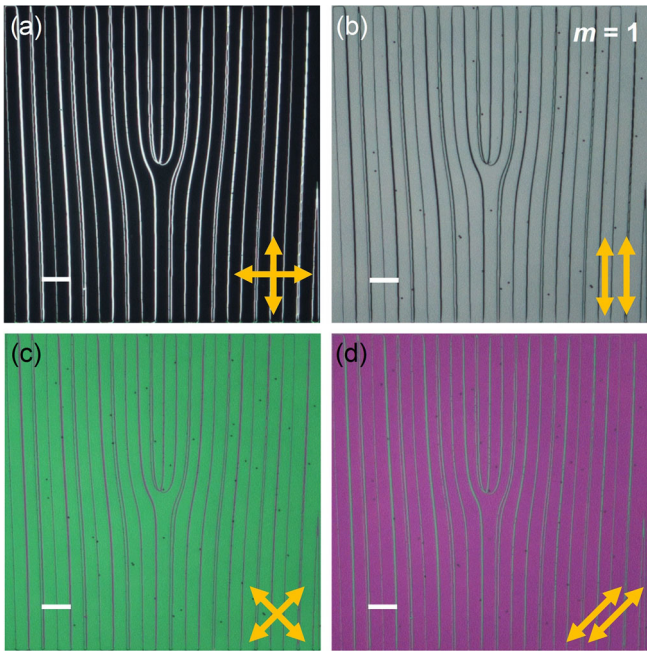

FIG. 2. Micrographs of the LC DVG with $m = 1$ recorded under a polarized optical microscope. The relative directions of the polarizer and analyzer are labeled in orange arrows. All scale bars are 100 μm.

A linearly polarized 632.8-nm laser illuminates the sample in Fig. 2 and the diffraction patterns are captured by a camera. As expected, there mainly exist five orders and the $\pm$1st, $\pm$2nd orders are donut-like OAM modes carrying topological charges of ±1, ±2, respectively. The dependency of the diffraction efficiency (η) on the applied voltages (V) is investigated. Here, η is defined as the intensity ratio of certain diffraction order to the total transmitted light. η-V curves of the 0th, $\pm$1st, and $\pm$2nd orders are plotted in Fig. 3(c). Along with the increase of V, according to Eq. (6), Γ decreases gradually towards zero as n_{eff} changes from n_e to n_o [39]. $\pm$1st and $\pm$2nd orders always change synchronously with similar efficiencies. At 1.6 V, $\Gamma = 2\pi$ and the diffraction is highly suppressed ($\eta_{\pm1} + \eta_{\pm2} = 3.3\% \pm 0.2\%$) and only the 0th order can be clearly observed (*off* state) as shown in Fig. 3(a). While at 1.2 and 2.5 V, Γ changes to 3π and π, respectively, and the LC DVG generates five equal-energy diffraction orders. Both $\pm$1st and $\pm$2nd orders can be clearly observed (*on* state) as shown in Fig. 3(b). At 2.5 V, $\eta_0 = 13.0\% \pm 0.2\%$, $\eta_{+1} = 16.8\% \pm 0.3\%$, $\eta_{-1} = 16.6\% \pm 0.3\%$, $\eta_{+2} = 13.8\% \pm 0.2\%$, and $\eta_{-2} = 13.4\% \pm 0.2\%$. The total efficiency is $\eta = 73.6\% \pm 0.5\%$, consistent with the theoretical value 77.4% [27]. The dependency of all five diffraction orders on the incident polarization at 2.5 V is plotted in Fig. 3(d). A half wave plate is utilized to alter the incident linear polarization from 0° to 360°. Their diffraction efficiencies are almost unchanged, verifying the excellent polarization independency to normally incident light.

Two examples of two-dimensional DVGs with $m = 1$ and 1 and $m = 1$ and 3 are exhibited in Figs. 4(a) and 4(b) and Fig. 4(c), respectively. The latter one has more fork fringes in y dimension. Figure 4(d) shows the diffraction pattern of the former sample at 632.8 nm. 5×5 diffraction orders (n_x, n_y) carrying topological charge $n_x m_x + n_y m_y$ (here, $m_x = m_y = 1$) are clearly observed. The detailed topological charge distribution is presented in Fig. 4(e). The efficiencies of high-order OAM modes are improved compared to conventional vortex gratings [14]. By electrically tuning, the phase retardation can reach π for a wide wavelength range. According to Eq. (6), for the LC E7 and $d = 6$ μm, we obtain $\lambda_{\text{max}} \approx 2.4$ μm. It is worth mentioning that the SD1 could be reoriented by blue or UV

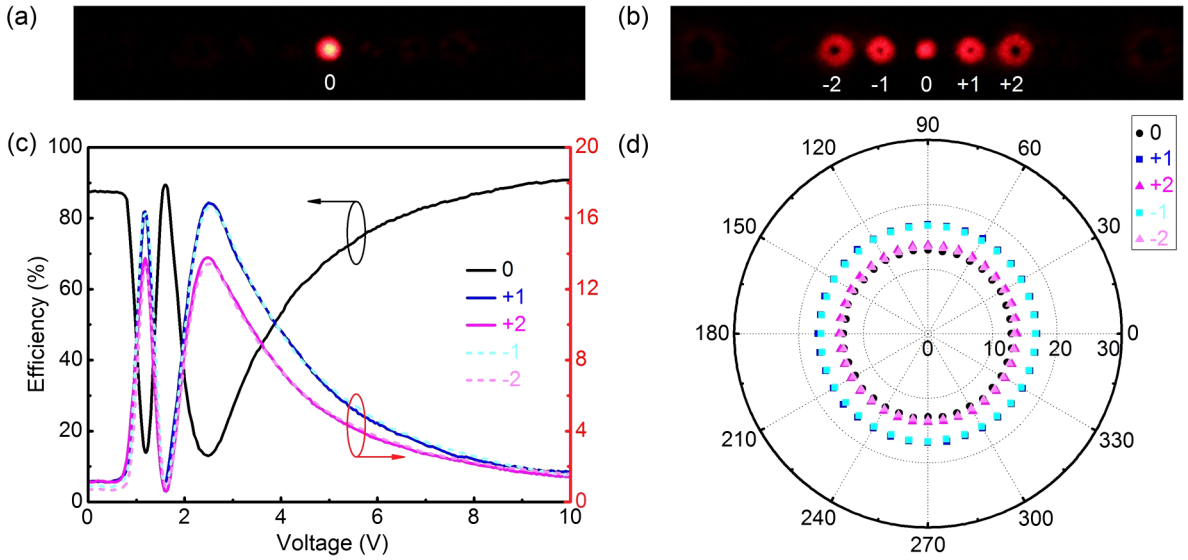

FIG. 3. The diffraction patterns of (a) *off* and (b) *on* states of the LC DVG. The dependencies of diffraction efficiency on (c) the applied voltage (corresponding vertical axes are indicated by arrows) and (d) the incident polarization at 2.5 V. The uncertainties of the experimental values of diffraction efficiencies in (c) and (d) are less than 0.3%.

light, which restricts its applications in the corresponding wavelength range. However, the problem could be solved by introducing inerasable alignment agents [41]. That means the device can operate at a range from green light to near infrared, for instance, equivalent diffraction property is also achieved at 532 nm for the same sample at 2.7 V as shown in Fig. 4(f).

In addition to the above simple OAM modes, more complex OAM modes carrying a fractional topological charge and nonzero radial index are also demonstrated. The phase pattern of a DVG with $m = 0.5$ is revealed in Fig. 5(a), featured by a radial phase dislocation corresponding to the fractional part of the topological charge [42]. A corresponding micrograph is shown in Fig. 5(b). The phase astride the radial discontinuity shifts half period for half integer, resulting in broken annular diffraction patterns as the first orders ($m = \pm 0.5$) exhibited in Fig. 5(c). Figure 5(d) shows the DVG phase pattern with $m = 1$ and $p = 1$, and a circular disclination is observed in Fig. 5(e) owing to the half-period shift of the phase pattern. A corresponding diffraction pattern is shown in Fig. 5(f). The first orders are biringed while the second orders have only a single ring ($m = \pm 2$ without p), as previously discussed.

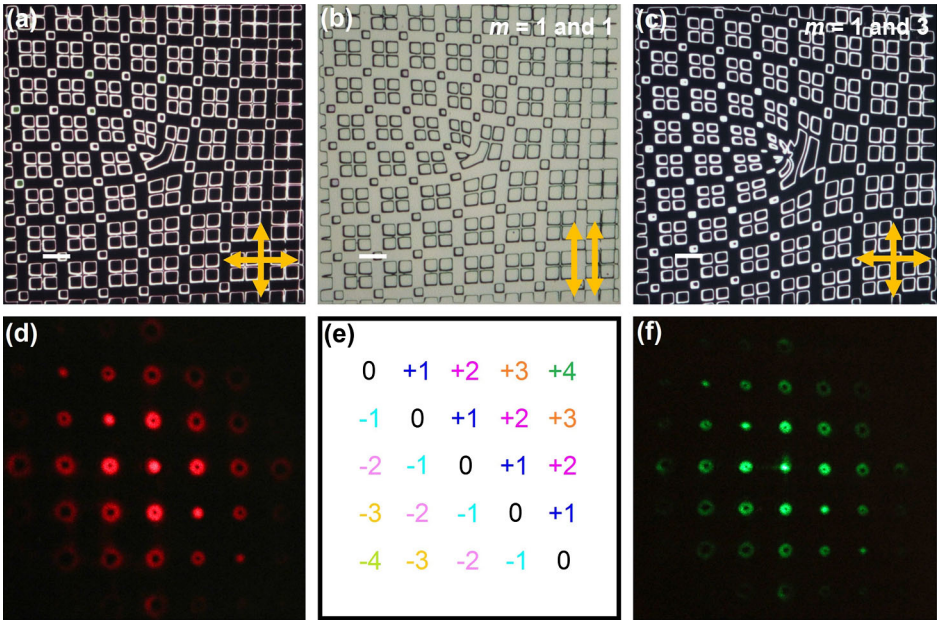

FIG. 4. Micrographs of 5×5 LC DVGs with (a),(b) $m = 1$ and 1 and (c) $m = 1$ and 3. The diffraction patterns of the sample (a) at wavelengths of incident light: (d) 632.8 nm and (f) 532 nm. The distribution of topological charges of (d) and (f) are presented in (e). All scale bars are 100 μm.

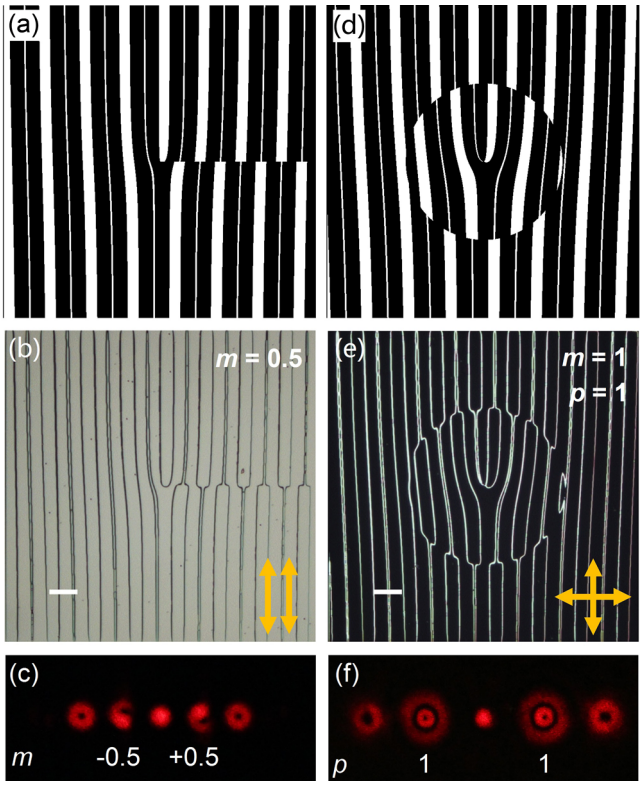

FIG. 5. The theoretical phase patterns of 1×5 LC DVGs with (a) $m = 0.5$ and (d) $m = 1$ and $p = 1$. The corresponding micrographs and diffraction patterns shown in (b),(c) and (e), (f), respectively. The topological charges or radial indices of the first orders are labeled. All scale bars are 100 μm.

Herein, only DVGs with five desired diffraction orders are presented as examples. Actually, the order number could be freely designed by selecting proper Dammann parameters. The energy distribution of different diffraction orders is slightly nonuniform. Some intensity distortion can be observed, which is caused by the imperfect structure of grating or phase singularity [43]. These could be attributed to the errors in the fabrication process and influence of the disclination lines. The above issues could be addressed via increasing the resolution of the exposure system and optimizing Dammann parameters. Besides the dynamic microlithography technology, other methods such as laser direct writing [44] can also be adopted to demonstrate the design. For the nematic LC E7 used here, the switching time is in the millisecond scale, which can be further improved to submillisecond, even tens of microsecond, by employing dual-frequency [40] or ferroelectric LC [45].

For parallel detection [19,21], when the illuminating beam is multihelix composed of OAM with charge $\{m_1, m_2, \ldots, m_m\}$, the same diffraction order n of the DVG with charge m will possess the superposition OAM modes with charge $\{nm + m_1, nm + m_2, \ldots, nm + m_m\}$. If among $\{m_1, m_2, \ldots, m_m\}$, there is one value of m_x satisfying $m_x + km = 0$, the wave function of the order k will possess a partial plane wave. In the far field, this is characterized by a central bright spot which can serve as the criteria for detection. Thanks to the relatively higher efficiencies of high-order OAM modes generated by DVGs, the detection range would be greatly extended (for example, a topological charge detection range from -12 to $+12$ was achieved in Ref. [20]). Additionally, OAM can be individually modulated without overlapping. Moreover, the applications of the proposed LC DVGs are not limited to OAM detection. Both fractional m and nonzero p LG modes, which have great potentials in quantum entanglement [46,47], cold atom trapping [48], and gravitational wave detection [30], are demonstrated by the Dammann concept encoded structures. The excellent mode variety may further extend the capability of optical communications and bring new opportunities to other fields.

IV. CONCLUSION

Photopatterned LC DVGs are proposed and demonstrated for the generation of various equal-energy OAM beams. They are composed of alternative orthogonal PA regions and realized by photopatterning a polarization-sensitive alignment agent through a dynamic microlithography system. A variety of OAM beams including integral or fractional m with and without p, as well as the two-dimensional OAM beam arrays, are generated in high efficiency and good quality. Excellent electrical switching, polarization independency, and wavelength tolerance are exhibited. This work supplies a universal and practical approach for OAM generation, manipulation, and detection.

ACKNOWLEDGMENTS

This work was supported by the NSFC programs (No. 11304151, No. 61490714, No. 61435008, and No. 61575093) and the Ph.D. Programs Foundation of the Ministry of Education of China (No. 20120091120020).

[1] G. Molina-Terriza, J. P. Torres, and L. Torner, Twisted photons, Nat. Phys. **3**, 305 (2007).
[2] S. Franke-Arnold, L. Allen, and M. Padgett, Advances in optical angular momentum, Laser Photonics Rev. **2**, 299 (2008).
[3] A. M. Yao and M. J. Padgett, Orbital angular momentum: Origins, behavior and applications, Adv. Opt. Photonics **3**, 161 (2011).
[4] B. Y. Wei, W. Hu, Y. Ming, F. Xu, S. Rubin, J. G. Wang, V. Chigrinov, and Y. Q. Lu, Generating switchable and reconfigurable optical vortices via photopatterning of liquid crystals, Adv. Mater. **26**, 1590 (2014).
[5] L. Allen, M. W. Beijersbergen, R. Spreeuw, and J. Woerdman, Orbital angular momentum of light and the transformation of Laguerre-Gaussian laser modes, Phys. Rev. A **45**, 8185 (1992).

[6] H. Kogelnik and T. Li, Laser beams and resonators, Appl. Opt. **5**, 1550 (1966).
[7] L. Paterson, M. MacDonald, J. Arlt, W. Sibbett, P. Bryant, and K. Dholakia, Controlled rotation of optically trapped microscopic particles, Science **292**, 912 (2001).
[8] M. Padgett and R. Bowman, Tweezers with a twist, Nat. Photonics **5**, 343 (2011).
[9] K. Toyoda, K. Miyamoto, N. Aoki, R. Morita, and T. Omatsu, Using optical vortex to control the chirality of twisted metal nanostructures, Nano Lett. **12**, 3645 (2012).
[10] Z. Zhu, W. Gao, C. Mu, and H. Li, Reversible orbital angular momentum photon-phonon conversion, Optica **3**, 212 (2016).
[11] V. D'Ambrosio, E. Nagali, S. P. Walborn, L. Aolita, S. Slussarenko, L. Marrucci, and F. Sciarrino, Complete experimental toolbox for alignment-free quantum communication, Nat. Commun. **3**, 961 (2012).
[12] D. S. Ding, W. Zhang, Z. Y. Zhou, S. Shi, G. Y. Xiang, X. S. Wang, Y. K. Jiang, B. S. Shi, and G. C. Guo, Quantum Storage of Orbital Angular Momentum Entanglement in an Atomic Ensemble, Phys. Rev. Lett. **114**, 050502 (2015).
[13] X. L. Wang, X. D. Cai, Z. E. Su, M. C. Chen, D. Wu, L. Li, N. L. Liu, C. Y. Lu, and J. W. Pan, Quantum teleportation of multiple degrees of freedom of a single photon, Nature (London) **518**, 516 (2015).
[14] G. Gibson, J. Courtial, M. Padgett, M. Vasnetsov, V. Pas'ko, S. Barnett, and S. Franke-Arnold, Free-space information transfer using light beams carrying orbital angular momentum, Opt. Express **12**, 5448 (2004).
[15] J. Wang, J. Y. Yang, I. M. Fazal, N. Ahmed, Y. Yan, H. Huang, Y. Ren, Y. Yue, S. Dolinar, M. Tur, and A. E. Willner, Terabit free-space data transmission employing orbital angular momentum multiplexing, Nat. Photonics **6**, 488 (2012).
[16] A. E. Willner, H. Huang, Y. Yan, Y. Ren, N. Ahmed, G. Xie, C. Bao, L. Li, Y. Cao, Z. Zhao, J. Wang, M. P. J. Lavery, M. Tur, S. Ramachandran, A. F. Molisch, N. Ashrafi, and S. Ashrafi, Optical communications using orbital angular momentum beams, Adv. Opt. Photonics **7**, 66 (2015).
[17] G. C. Berkhout, M. P. Lavery, J. Courtial, M. W. Beijersbergen, and M. J. Padgett, Efficient Sorting of Orbital Angular Momentum States of Light, Phys. Rev. Lett. **105**, 153601 (2010).
[18] M. Mirhosseini, M. Malik, Z. Shi, and R. W. Boyd, Efficient separation of the orbital angular momentum eigenstates of light, Nat. Commun. **4**, 2781 (2013).
[19] T. Lei, M. Zhang, Y. R. Li, P. Jia, G. N. Liu, X. G. Xu, Z. H. Li, C. J. Min, J. Lin, C. Y. Yu, H. B. Niu, and X. C. Yuan, Massive individual orbital angular momentum channels for multiplexing enabled by Dammann gratings, Light Sci. Appl. **4**, e257 (2015).
[20] N. Zhang, X. Yuan, and R. Burge, Extending the detection range of optical vortices by Dammann vortex gratings, Opt. Lett. **35**, 3495 (2010).
[21] Z. Wang, N. Zhang, and X. C. Yuan, High-volume optical vortex multiplexing and de-multiplexing for free-space optical communication, Opt. Express **19**, 482 (2011).
[22] J. Yu, C. Zhou, W. Jia, J. Wu, L. Zhu, Y. Lu, C. Xiang, and S. Li, Generation of controllable rotating petal-like modes using composited Dammann vortex gratings, Appl. Opt. **54**, 1667 (2015).
[23] I. Moreno, J. A. Davis, D. M. Cottrell, N. Zhang, and X. C. Yuan, Encoding generalized phase functions on Dammann gratings, Opt. Lett. **35**, 1536 (2010).
[24] J. Yu, C. Zhou, Y. Lu, J. Wu, L. Zhu, and W. Jia, Square lattices of quasi-perfect optical vortices generated by two-dimensional encoding continuous-phase gratings, Opt. Lett. **40**, 2513 (2015).
[25] H. Dammann and K. Görtler, High-efficiency in-line multiple imaging by means of multiple phase holograms, Opt. Commun. **3**, 312 (1971).
[26] H. Dammann and E. Klotz, Coherent optical generation and inspection of two-dimensional periodic structures, Opt. Acta **24**, 505 (1977).
[27] C. Zhou and L. Liu, Numerical study of Dammann array illuminators, Appl. Opt. **34**, 5961 (1995).
[28] R. Vinu, M. K. Sharma, R. K. Singh, and P. Senthilkumaran, Generation of spatial coherence comb using Dammann grating, Opt. Lett. **39**, 2407 (2014).
[29] P. Chen, B. Y. Wei, W. Ji, S. J. Ge, W. Hu, F. Xu, V. Chigrinov, and Y. Q. Lu, Arbitrary and reconfigurable optical vortex generation: A high-efficiency technique using director-varying liquid crystal fork gratings, Photonics Res. **3**, 133 (2015).
[30] M. Granata, C. Buy, R. Ward, and M. Barsuglia, Higher-Order Laguerre-Gauss Mode Generation and Interferometry for Gravitational Wave Detectors, Phys. Rev. Lett. **105**, 231102 (2010).
[31] N. Matsumoto, T. Ando, T. Inoue, Y. Ohtake, N. Fukuchi, and T. Hara, Generation of high-quality higher-order Laguerre-Gaussian beams using liquid-crystal-on-silicon spatial light modulators, J. Opt. Soc. Am. A **25**, 1642 (2008).
[32] J. Yu, C. Zhou, W. Jia, A. Hu, W. Cao, J. Wu, and S. Wang, Three-dimensional Dammann vortex array with tunable topological charge, Appl. Opt. **51**, 2485 (2012).
[33] W. Hu, A. K. Srivastava, X. W. Lin, X. Liang, Z. J. Wu, J. T. Sun, G. Zhu, V. Chigrinov, and Y. Q. Lu, Polarization independent liquid crystal gratings based on orthogonal photoalignments, Appl. Phys. Lett. **100**, 111116 (2012).
[34] M. Schadt, K. Schmitt, V. Kozinkov, and V. Chigrinov, Surface-induced parallel alignment of liquid crystals by linearly polymerized photopolymers, Jpn. J. Appl. Phys. **31**, 2155 (1992).
[35] H. Wu, W. Hu, H. C. Hu, X. W. Lin, G. Zhu, J. W. Choi, V. Chigrinov, and Y. Q. Lu, Arbitrary photo-patterning in liquid crystal alignments using DMD based lithography system, Opt. Express **20**, 16684 (2012).
[36] V. Chigrinov, S. Pikin, A. Verevochnikov, V. Kozenkov, M. Khazimullin, J. Ho, D. D. Huang, and H. S. Kwok, Diffusion model of photoaligning in azo-dye layers, Phys. Rev. E **69**, 061713 (2004).
[37] B. Y. Wei, P. Chen, W. Hu, W. Ji, L. Y. Zheng, S. J. Ge, Y. Ming, V. Chigrinov, and Y. Q. Lu, Polarization-controllable Airy beams generated via a photoaligned director-variant liquid crystal mask, Sci. Rep. **5**, 17484 (2015).
[38] P. Chen, W. Ji, B. Y. Wei, W. Hu, V. Chigrinov, and Y. Q. Lu, Generation of arbitrary vector beams with liquid crystal polarization converters and vector-photoaligned *q*-plates, Appl. Phys. Lett. **107**, 241102 (2015).

[39] I. C. Khoo and S. T. Wu, *Optics and Nonlinear Optics of Liquid Crystals* (World Scientific, Singapore, 1993).
[40] X. W. Lin, W. Hu, X. K. Hu, X. Liang, Y. Chen, H. Q. Cui, G. Zhu, J. N. Li, V. Chigrinov, and Y. Q. Lu, Fast response dual-frequency liquid crystal switch with photo-patterned alignments, Opt. Lett. **37**, 3627 (2012).
[41] M. Schadt and H. Seiberle, Optical patterning of multi-domain LCDs, J. Soc. Inf. Disp. **5**, 367 (1997).
[42] J. Leach, E. Yao, and M. J. Padgett, Observation of the vortex structure of a non-integer vortex beam, New J. Phys. **6**, 71 (2004).
[43] Y. Liu, X. Ling, X. Yi, X. Zhou, S. Chen, Y. Ke, H. Luo, and S. Wen, Photonic spin Hall effect in dielectric metasurfaces with rotational symmetry breaking, Opt. Lett. **40**, 756 (2015).
[44] J. Kim, Y. Li, M. N. Miskiewicz, C. Oh, M. W. Kudenov, and M. J. Escuti, Fabrication of ideal geometric-phase holograms with arbitrary wavefronts, Optica **2**, 958 (2015).
[45] Y. Ma, B. Y. Wei, L. Y. Shi, A. K. Srivastava, V. G. Chigrinov, H. S. Kwok, W. Hu, and Y. Q. Lu, Fork gratings based on ferroelectric liquid crystals, Opt. Express **24**, 5822 (2016).
[46] S. Oemrawsingh, X. Ma, D. Voigt, A. Aiello, E. Eliel, and J. Woerdman, Experimental Demonstration of Fractional Orbital Angular Momentum Entanglement of Two Photons, Phys. Rev. Lett. **95**, 240501 (2005).
[47] L. Chen, J. Lei, and J. Romero, Quantum digital spiral imaging, Light Sci. Appl. **3**, e153 (2014).
[48] M. Clifford, J. Arlt, J. Courtial, and K. Dholakia, High-order Laguerre–Gaussian laser modes for studies of cold atoms, Opt. Commun. **156**, 300 (1998).